Journal of Nanobiotechnology

RESEARCH

Open Access

Biomimetic gene delivery system coupled with extracellular vesicle–encapsulated AAV for improving diabetic wound through promoting vascularization and remodeling of inflammatory microenvironment

Shan He[1†], Zhenhao Li[1,4†], Lei Xie[5†], Rongtian Lin[6†], Biying Yan[3,9†], Bixiang Li[7], Lingxi Luo[7], Youshan Xv[8], Huangding Wen[1], Yaxuan Liang[3,9*], Cong Huang[2*] and Zhiqing Li[1*]

Abstract

Adeno-associated virus (AAV)-mediated gene transfer has demonstrated potential in effectively promoting re-epithelialization and angiogenesis. AAV vector has a safety profile; however, the relatively low delivery efficacy in chronic wound with an inflammatory microenvironment and external exposure has limited its prospective clinical translation. Here, we generated AAV-containing EVs (EV-AAVs) from cultured HEK 293T cells and confirmed that the gene transfer efficiency of VEGF-EV-AAV significantly surpassed that of free AAV. Subsequently, a biomimetic gene delivery system VEGF-EV-AAV/MSC-Exo@FHCCgel developing, and synergistically enhances anti-inflammation and transfection efficiency in the combination of human umbilical cord mesenchymal stem cell-derived exosomes (hUC-MSC-Exo). Upon reaching physiological temperature, this hydrogel system transitions to a gel state, maintaining AAV bioactivity and facilitating a sustained release of the encapsulated vesicles. The encapsulation strategy enables the vesicles to rapidly fuse with endothelial cell membranes, ensuring controlled expression of endogenous VEGF. Results revealed that VEGF-EV-AAV/MSC-Exo@FHCCgel alleviates mitochondrial function in endotheliocyte under oxidative stress. Furthermore, it eliminates senescent macrophages by inhabitation of cyclic GMP-AMP (cGAMP) synthase (cGAS)-stimulator of interferon genes (STING) pathway to promote efferocytosis. The system increases Treg cells accumulation, leading to a reduction of inflammatory cytokines. Collectively, the biomimetic gene delivery system represents a promising multi-faceted strategy for chronic wound healing.

†Shan He, Zhenhao Li, Lei Xie, Rongtian Lin and Biying Yan contributed equally to this work.

*Correspondence:
Yaxuan Liang
y.liang@bnu.edu.cn
Cong Huang
chuang200628@163.com
Zhiqing Li
lizq@smu.edu.cn

Full list of author information is available at the end of the article

Keywords Gene delivery, Adeno-associated virus, Extracellular vesicle, Diabetic wound, Inflammatory microenvironment

Introduction

Normal skin serves as a protective barrier covering the human body, vital for resisting external pathogens and adapting to environmental changes [1]. It plays a crucial role in maintaining homeostasis. In diabetic patients, the anatomical and functional integrity of the skin is compromised [2], disrupting the sequential phases of hemostasis, inflammation, proliferation, and remodeling necessary for normal wound healing [3]. The orderly regulation of angiogenesis and coordinated control of inflammatory responses are key to promoting proper wound healing, as excessive inflammatory conditions often lead to problematic vascularization and abnormal granulation tissue formation, ultimately manifesting as delayed healing [4]. Studies indicate that vascular endothelial growth factor (VEGF) is the most potent mitogen in the growth factor family for endothelial cells, facilitating endothelial proliferation and accelerating granulation tissue formation. Its involvement in vascular regeneration is beneficial for efficient wound repair [5]. VEGF holds a unique position in wound healing research as a critical regulator of angiogenesis [6]. Thus, enhancing VEGF expression in the wound microenvironment is essential for promoting chronic wound healing. Recent studies have focused on supplementing VEGF to aid wound healing, but exogenous growth factors struggle with precision control synchronized with the repair state. In contrast, the supplementation of endogenous VEGF offers superior controllability. Additionally, intracellularly produced VEGF can improve endothelial cell apoptosis and enhance survival in inflammatory environments [7, 8].

With the rapid advancement of gene engineering, gene therapy has become an effective method for sustained local effects of endogenous growth factors [9]. Adeno-associated virus (AAV) is a promising gene delivery vector for its safety, low toxicity, and multiple serotypes with preferred tropism to distinct tissue and cell types [10, 11]. To date, clinical trials of gene therapy have focused on targeting muscular tissues [12], retina [13], myocardium [14, 15], or tumor [16] via the delivery of specific nucleotides for protein expression and correction. However, the strategy for wound treatment via AAV remained complex and challenging. A major obstacle is the loss of vectors due to antibody neutralization and the impaired gene transfer efficacy [17]. Studies have shown that EVs collected from AAV-producing HEK293T cultures carry and deliver intact AAVs to the retina, inner ear, liver, and nervous system of mice [18]. With the rapid development of biomaterials, various implantable biomimetic engineering scaffolds for wound repair have been reported. To address the issues of inactivation and loss, this study proposes, for the first time, the construction of a biomimetic gene delivery system as a non-surgical therapy with significant potential for diabetic wound repair. The thermosensitive hydrogel system of the biomimetic scaffold enables the uniform dispersion of both hydrophilic and hydrophobic liposomes (MSC-Exo and VEGF-EV-AAV) within the matrix while maintaining activity, and can deliver them in any shape at the wound site [19, 20]. More importantly, it resolves the initial burst and uncontrollable release issues present in other hydrogel systems [21].

To correct the local inflammatory microenvironment of diabetic wounds [22] and further promote endothelial cell proliferation involved in vascularization [23], exosomes derived from human umbilical cord mesenchymal stem cells (hUC-MSC-Exo) were added. In recent years, hUC-MSC-Exo has been shown to have therapeutic potential for inflammatory [24] and aging diseases [25] and has become a non-cellular therapeutic nanomedicine [26]. Mesenchymal stem cells (MSCs) offer a versatile therapeutic platform for accelerating wound recovery and repair by comprehensively modulating the immune system [27] and promoting intercellular synergy [28]. On one hand, MSCs secrete anti-inflammatory cytokines [29] such as IL-10 and TGF-β, as well as inhibitors of pro-inflammatory cytokines, aiding in the regulation of the local inflammatory environment. On the other hand, exosomes released by MSCs can repair macrophage efferocytosis impairment [30], thus participating in immune modulation.

This study, based on iodixanol ultracentrifugation, obtained highly purified vesicles encapsulating adenoviruses (VEGF-EV-AAV) as a natural envelope, protecting the carried VEGF gene sequences and facilitating rapid uptake by endothelial cells through phagocytosis, ensuring efficient transfection, and sustained progeny expression of endogenous VEGF. Additionally, a thermosensitive hydrogel-based biomimetic gene delivery system, VEGF-EV-AAV/MSC-Exo@FHCCgel, was designed to co-deliver MSC-Exo and VEGF-EV-AAV, synergistically remodeling the inflammatory microenvironment (Scheme 1). The gene delivery system elucidates the cascade regulatory mechanisms between promoting endothelial cell proliferation, improving macrophage senescence, and regenerating basal blood vessels. By eliminating macrophages senescence and inducing macrophages efferocytosis and promoting Treg cell-mediated tissue repair, this bioresponsive strategy versatilely

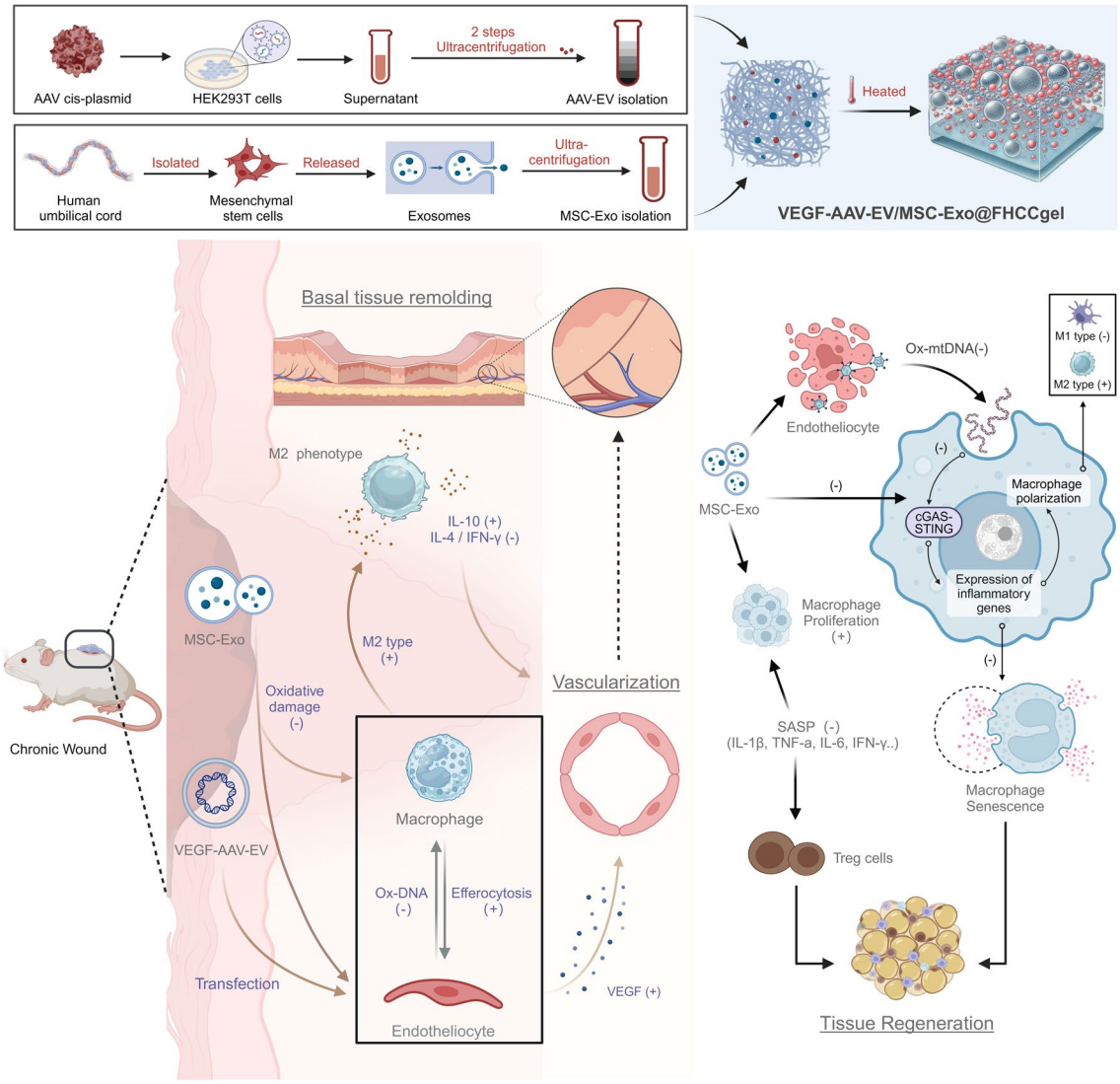

Scheme 1 VEGF-EV-AAV/MSC-Exo@FHCCgel construction and synergistic effect of reshaping the inflammatory microenvironment

reshaping the inflammatory microenvironment, is an attractive approach for diabetic wound healing.

Results and discussion

Density gradient ultracentrifugation purification successfully enriched EV-AAVs

Our overarching objective was to isolate and thoroughly characterize highly purified EV-AAVs, assessing their efficacy in delivering VEGF to HUVECs (Fig. 1a). HEK293T cells, approved by the FDA for AAV production and known for EV secretion, have been extensively utilized. Previous studies indicated that HEK293T cells producing AAV naturally secreted EV-AAVs into the culture medium. Three-dimensional fluorescence analysis showed that within 72 h, mCherry-AAV successfully self-assembled within HEK293T cells expressing the mCherry red fluorescent protein (Fig. 1b). In practice, besides the required EV-AAV, the supernatant contained a mixture of numerous free AAVs and simple EVs. To isolate EV-AAVs free of free AAV contamination, we innovatively designed a stepwise protocol using a 15–60% iodixanol density gradient, from which purified EV-AAV particles were collected. Target EV-AAVs were primarily located in fraction F6 (highlighted in gray). Tetraspanin protein expression on the EV surface was analyzed via flow cytometry (FC), showing no difference between EV-AAV and EV (Fig. 1c). The quantity of AAVs was determined by qPCR (Fig. 1d). Furthermore, exosome marker proteins CD9 and CD63 were analyzed by western blotting (WB) (Fig. 1e and Figure S1). These strategies confirmed that the density gradient-based isolation strategy was highly effective in purifying EV-AAVs. To determine the size of different vesicles, dynamic light scattering (DLS) was employed, revealing approximate sizes of EV-AAVs,

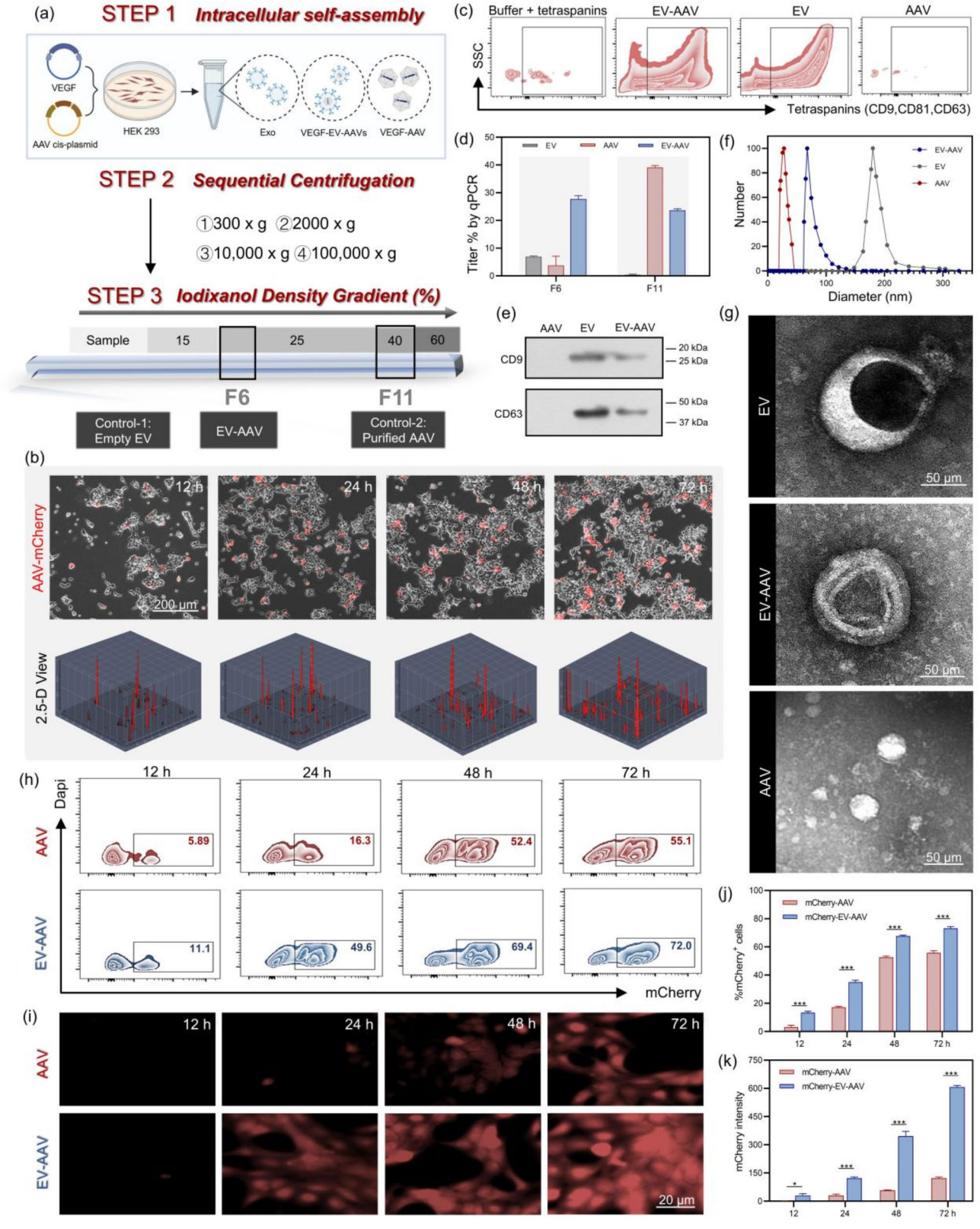

Fig. 1 (See legend on next page.)

(See figure on previous page.)

Fig. 1 Characterization of purified EV-AAV. (**a**) Synthesis of EV-AAV through iodixanol-based high-speed centrifugation. (**b**) Time-dependent expression of mCherry fluorescence in HEK293T cells and analysis using a 2.5-Dimensional visualization technique. (**c**) Surface characterization of EV-AAV, EV, and AAV via nano-flow cytometry for tetraspanin proteins CD9 and CD63, with buffer plus tetraspanin serving as the gating control. Identification of EV-AAV, AAV, and EV confirmed by (**d**) quantitative PCR and (**e**) Western blot analysis. (**f**) Hydrodynamic size distribution of extracellular vesicle-encapsulated adeno-associated vectors (EV-AAV), isolated EVs, and free AAV particles. (**g**) Transmission electron microscopy (TEM) provided representative images showcasing extracellular vesicle-encapsulated adeno-associated vectors (EV-AAV), isolated EVs, and free AAV particles. Functional assessment of cellular uptake and expression included (**h**) flow cytometry and (**i**) CLSM of HUVECs at three days post-infection with equivalent titers of mCherry-tagged EV-AAV and mCherry-AAV. (**j**) Quantification of mCherry-positive HUVECs via flow cytometry. (**k**) Confocal microscopy analysis of mCherry fluorescence intensity in HUVECs, presented as median values with ranges and analyzed using the Mann-Whitney U test, indicating statistical significance where $*P < 0.05$. Experiments were biologically replicated thrice, with representative outcomes displayed

EVs, and AAVs as 100 nm, 180 nm, and 20 nm, respectively (Fig. 1f). Additionally, ultrathin sections of the three types of vesicles were processed and imaged using transmission electron microscopy, where AAVs encapsulated within EV-AAVs were observed (Fig. 1g).

To compare the gene transfer efficiencies of AAV and EV-AAV, equititered mCherry-AAV and mCherry-AAV were co-incubated with HUVECs at 37 °C. The transduction efficiency of the vectors was assessed via FC (Fig. 1h) and CLSM quantifying mCherry expression (Fig. 1i). Results analysis (Fig. 1j-k) indicated that the transduction efficiency of EV-AAV was significantly higher than that of AAV. This enhancement is likely due to the outer vesicular membrane's similarity to cellular membranes, facilitating cellular uptake via endocytosis [31], thereby accelerating the transfection process and enhancing efficiency.

Characterization of VEGF-EV-AAV/MSC-E Xo@FHCCgel

Due to the vesicles being loaded as liposomes, the thermosensitive hydrogel can overcome the defect of pre-curing damage to biological activity inherent in traditional hydrogel systems [32]. Additionally, in situ curing allows perfect conformity to wound surfaces and addresses the burst release issue of liposomes [33]. For this purpose, we prepared a thermosensitive hydrogel (FHCCgel) based on F127 as a tissue engineering scaffold for gene delivery systems. Upon incubation in a 37 °C water bath, the hydrogel was observed to solidify (Fig. 2a). Post-solidification and freeze-drying, SEM revealed a uniformly porous three-dimensional network structure within the VEGF-EV-AAV/MSC-Exo@FHCCgel (Fig. 2b). Based on the results from the scanning electron microscopy (SEM), tensile stress, and elastic modulus, the structure became more porous and loose after the addition of chitosan, with increased pore size (Figure S3). To assess degradation periods, a defined volume of the solidified hydrogel was placed in PBS (pH 7.4, 37 °C) and in an oxidative alkaline environment mimicking diabetic wound surfaces (pH 8.0). The process was maintained in a constant temperature water bath at 37 °C, with periodic removal for drying and weighing, resulting in calculated degradation periods of 10 and 14 days, respectively (Fig. 2c). In addition, we confirmed that the VEGF-EV-AAV/MSC-Exo@FHCCgel can be completely degraded in vivo, with no significant residual material observed (Figure S4). Although the degradation period was shortened under simulated conditions, it still contributed to early substrate vascularization processes (7 days). As shown in Fig. 2d, the thermosensitive hydrogel in PBS solution gradually released VEGF-EV-AAV and MSC-Exo in 7 days.

Biocompatible F127, approved by the FDA for use as a temperature-sensitive curable agent, produced a hydrogel with less-than-ideal mechanical strength [34]. Wound dressings often need to provide a certain rigidity to support the internal three-dimensional structure, which is beneficial for the migration and attachment of repair cells around the wound. Compared to the curing speed of the gel, the loading of liposomes focuses more on temperature control to maintain biological activity. Adjuvants such as HPMC-100 M were used effectively to adjust Tgel [35], while chitosan and type I collagen enhanced gel strength and biocompatibility through self-assembling cross-linked networks. Thus, these components were mixed with F127 in specific proportions (18% F127, 0.5% HPMC-100 M, 0.25% chitosan, 0.25% type I collagen) to prepare the thermosensitive hydrogel (FHCCgel). Tgel was measured at 37.0 °C (Fig. 2e). The value of EV-AAV MOI in the control gene delivery system is 1. Human umbilical cord MSCs exosomes (abbreviation, MSC-Exo) were prepared as described in previous studies, and characterization confirmed successful extraction to MSC-Exo (Figure S2) [36]. The EV-AAV and MSC-Exo were mixed in a 1:1 ratio to participate in the preparation of the gene delivery system. In Fig. 2f, mCherry-EV-AAV/MSC-Exo@FHCCgel and mCherry-AAV/MSC-Exo@FHCCgel were implanted into murine wound sites, with IVIRS observing sustained in vivo enhancement of fluorescent proteins, the former showing higher transfection efficiency (Fig. 2g). These results demonstrate that the gene delivery system based on FHCCgel can simultaneously maintain biological activity and mechanical rigidity.

Biocompatibility evaluation

As for implantable biomaterials, it is imperative that excellent biocompatibility and absence of cytotoxicity are thoroughly validated. Results from the LDH assay

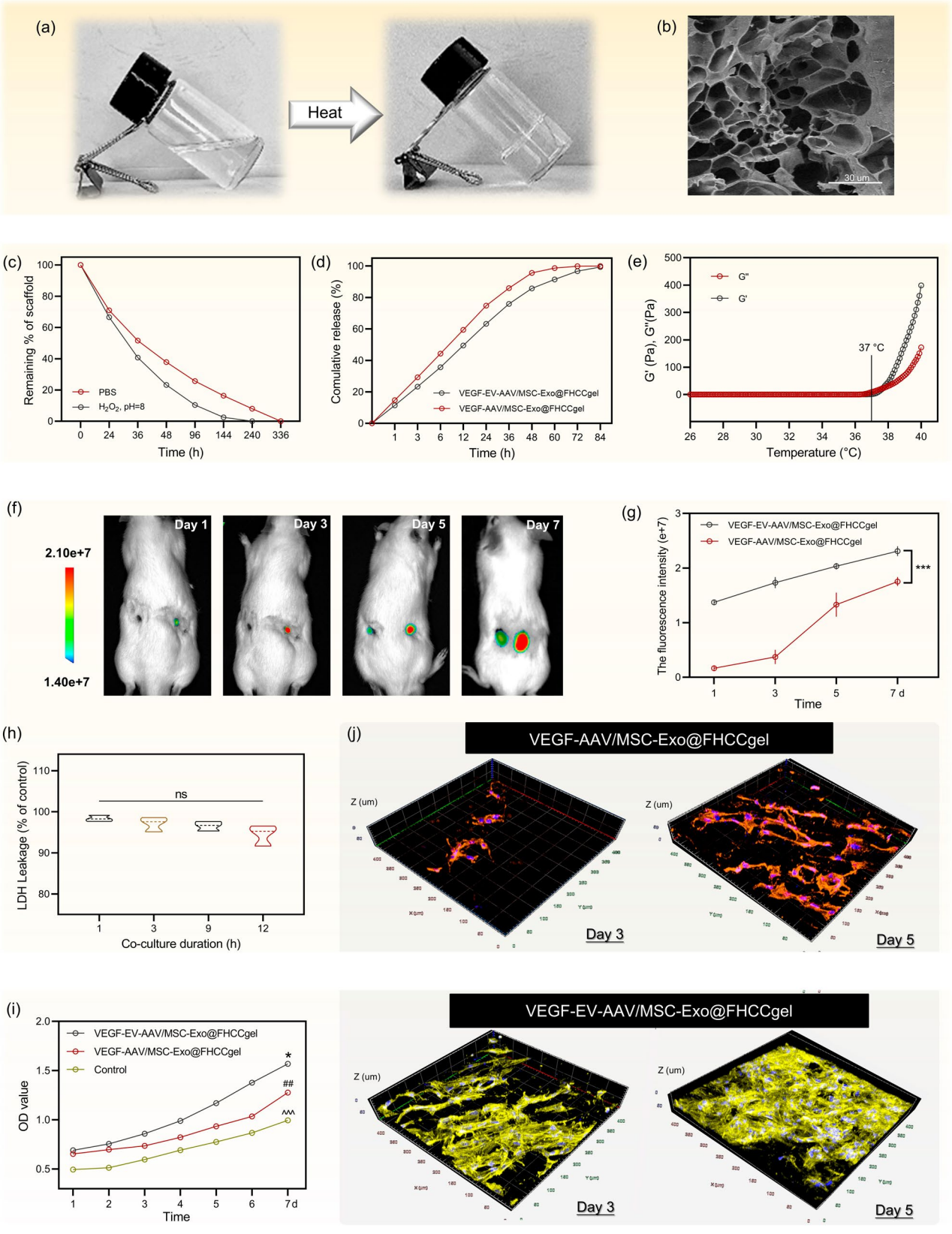

Fig. 2 (See legend on next page.)

(See figure on previous page.)

Fig. 2 Development of a thermosensitive 3D scaffold VEGF-EV-AAV/MSC-Exo@FHCCgel for controlled delivery. (**a**) Visual confirmation of the temperature-induced gelation of the hydrogel system. (**b**) SEM representation of the VEGF-EV-AAV/MSC-Exo@FHCCgel structure. (**c**) Depiction of the degradation kinetics, showing the percentage of remaining mass under various conditions over time. (**d**) Release kinetics of PKH26-labelled VEGF-EV-AAV and VEGF-AAV, expressed as cumulative percent release at sequential time intervals. (**e**) Temperature-dependent rheological properties, detailing storage modulus (G') and loss modulus (G"). (**f**) Infrared-visible reflectance spectroscopy (IVIRS) images demonstrating the transfection efficiency of fluorescent proteins in wounds treated with mCherry-EV-AAV/MSC-Exo@FHCCgel (right) versus mCherry-AAV/MSC-Exo@FHCCgel (left), with (**g**) corresponding fluorescence intensity measurements. (**h**) Lactate dehydrogenase (LDH) release assay quantifying cellular damage in HUVECs co-cultured with VEGF-EV-AAV/MSC-Exo@FHCCgel. (**i**) MTT assay results at designated time points post-treatment with VEGF-EV-AAV/MSC-Exo@FHCCgel, showing statistically significant differences: $^{*}p < 0.05$ for VEGF-EV-AAV/MSC-Exo@FHCCgel vs. VEGF-AAV/MSC-Exo@FHCCgel; $^{\#\#}p < 0.01$ for VEGF-AAV/MSC-Exo@FHCCgel vs. Control; $^{\wedge\wedge\wedge}p < 0.01$ for VEGF-EV-AAV/MSC-Exo@FHCCgel vs. Control. Data are presented as mean ± standard deviation. (**j**) Three-dimensional confocal laser scanning microscopy (3D-CLSM) images on days 3 and 5 showing the architecture of tissue-engineered dermis employing VEGF-EV-AAV/MSC-Exo@FHCCgel and VEGF-AAV/MSC-Exo@FHCCgel

(Fig. 2h), MTT (Fig. 2i) and CCK-8 assay (Figure S5a) indicated that there is no significant cytotoxicity in HaCaT, HUVEC, and L929 cells. The biocompatibility was evidenced by the no distinct damage of vital organs for the treated mice. Furthermore, negligible variations in the blood hematological assay also confirmed the excellent biosafety. (Figure S5b and c). To further assess the impact of the post-curing internal three-dimensional structure on cell migration and adhesion, cells seeded on the scaffold surface were able to migrate and adhere internally. Interestingly, the spreading and proliferation of cells within the VEGF-EV-AAV/MSC-Exo@FHCCgel were notably superior to those in the VEGF-AAV/MSC-Exo@FHCCgel (Fig. 2j). This suggests that VEGF-EV-AAV plays a significant role in enhancing endothelial cell migration and proliferation.

Anti-inflammatory influence in endotheliocytes through mitochondrial function recovery

Excessive reactive oxygen species (ROS) has been confirmed to cause damage on the mitochondria of Endothelial Cell (ECs) [37]. Repairing mitochondrial oxidative damage duly is critical for the normal physiological activity in endothelial cells [38]. Observed under biological-transmission electron microscopy (Bio-TEM), it has been further validated that VEGF-EV-AAV/MSC-Exo@FHCCgel can relieve the effects of H_2O_2 on mitochondria. Electron microscopy examination revealed that control group contains mitochondria in rod shapes with well-organized. In H_2O_2-treated HUVECs, mitochondrial shrinkage and blurred structure of inner membrane were observed, whereas the mitochondria in the VEGF-EV-AAV/MSC-Exo@FHCCgel group were nearly identical to those in the normal group in terms of intracellular mitochondrial structure (Fig. 3a). The timely closure of mitochondrial permeability transition pores (mPTP) and the maintenance of mitochondrial membrane potential ($\Delta\Psi m$) are crucial for sustaining cellular metabolism and proliferation [39, 40]. As one biological marker, mitochondrial function was shown by the red/green fluorescence intensity analysis (Fig. 3b) and FC (Fig. 3c) via JC-1 assay kit. Quantitative analysis in Fig. 3f suggested that HUVECs co-cultured with VEGF-EV-AAV/MSC-Exo@FHCCgel exhibited stronger red fluorescence (JC-1 aggregation) within mitochondria. While the effects were less pronounced, co-cultures with VEGF-EV-AAV@FHCCgel and MSC-Exo@FHCCgel similarly facilitated the recovery of mitochondrial function.

It is well-known that mitochondria possesses own DNA (mtDNA), which is a set of genetic instructions completely independent of nuclear DNA [41]. Through colocalization of 8-OHdG (oxidized mitochondrial DNA, Ox-mtDNA) with mitochondrial fluorescence, representative CLSM images demonstrated that co-culture with VEGF-EV-AAV/MSC-Exo@FHCCgel significantly reduced the presence of Ox-mtDNA (Fig. 3d and g). The mtDNA remains within mitochondria to maintains mitochondrial and cellular health; however, extracellular leakage of Ox-mtDNA through mitochondrial membrane pores (mPTP) can act as pathogen-associated molecular patterns (DAMPs), triggering an immune response and inducing inflammation [42]. Currently, excessive opening of mPTP is considered to activate pathophysiological processes by causing cellular and mitochondrial oxidation imbalances [43]. With calcein released from mitochondria due to excessive mPTP opening, the fluorescence was quenched by cobalt chloride, thus the accumulation of calcein selectively within mitochondria indicates the degree of opening. CLSM results showed that under oxidative condition, co-culture with VEGF-EV-AAV/MSC-Exo@FHCCgel reduced the opening rate of mPTP more effectively than other groups (Fig. 3e and h). We also conducted a long-term evaluation of the dynamics of mPTP using flow cytometry to assess the sustained impact of the material on mitochondrial recovery over a period of 72 h. During this process, an increasing number of mPTPs returned to a closed state (Figure S6).

Decrease of macrophage senescence based on the cGAS–STING pathway facilitates efferocytosis recovery

In this study, we further investigated the Møs senescence and polarization regulation of VEGF-EV-AAV/MSC-Exo@FHCCgel, within an oxidative microenvironment,

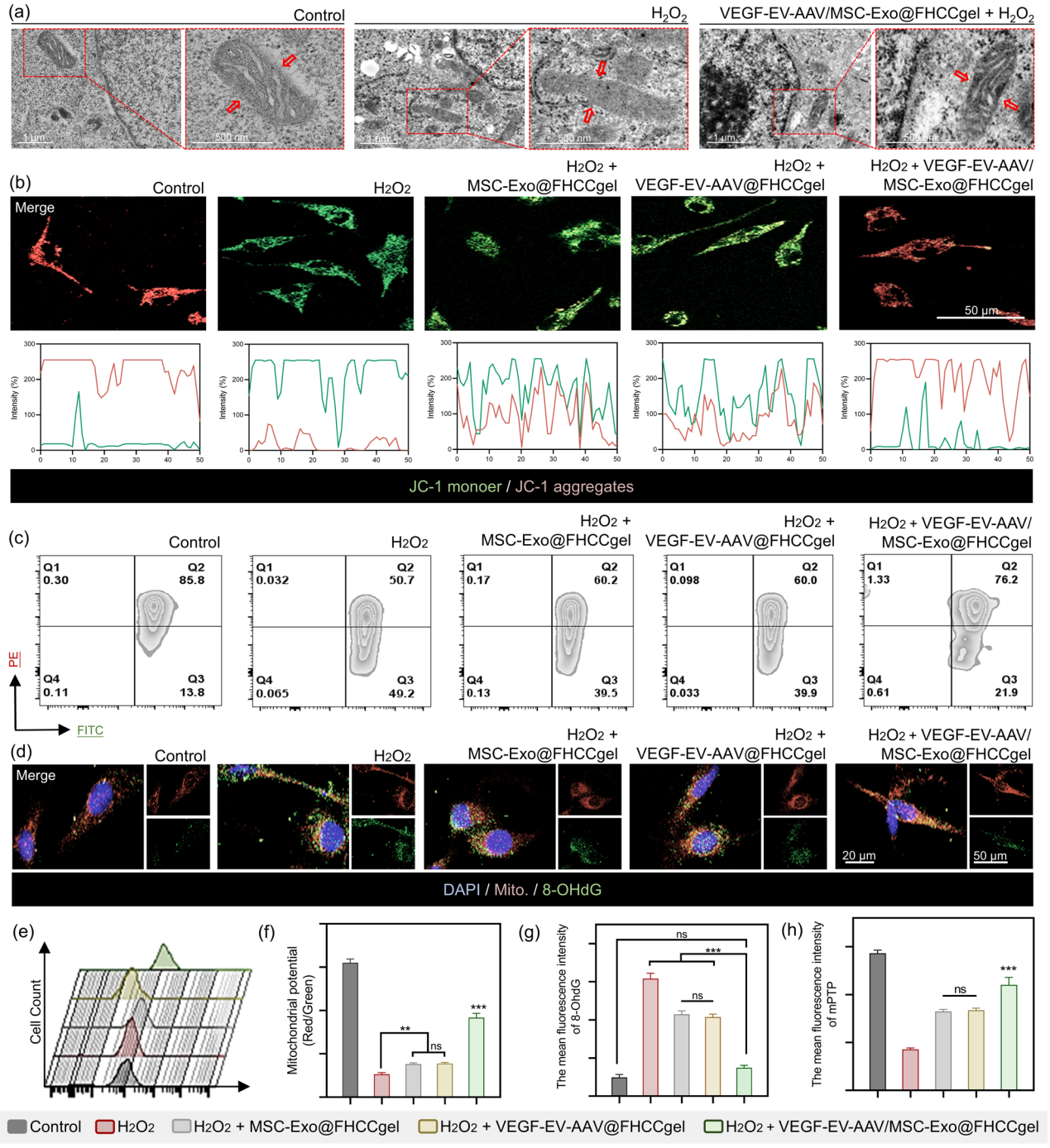

Fig. 3 Anti-inflammatory influence of VEGF-EV-AAV/MSC-Exo@FHCCgel on endothelial cells (HUVECs). (**a**) Bio-TEM analysis of ECs, illustrating the morphological alterations in mitochondria. (**b**) Representative confocal laser scanning microscopy (CLSM) images and (**c**) flow cytometry (FC) evaluation of mitochondrial membrane potential in HUVECs, red for JC-1 aggregates and green for JC-1 monomer. (**d**) CLSM imaging to detect 8-OHDG in mitochondria. (**e**) Post-treatment FC analysis for mitochondrial permeability transition pore (mPTP) in HUVECs. (**f**) The corresponding analysis of mitochondrial membrane potential. Statistical assessments of (**g**) 8-OHDG and (**h**) mPTP levels are shown. Error bars signify mean ± standard deviation, with a sample size of $n = 3$. Statistical notations include: n.s.=not significant, $^{**}p < 0.01$, $^{***}p < 0.001$, reflecting statistical significance

and its overall impact on the inflammatory state. As the Fig. 4a shown, endothelial cells (HUVECs) culture supernatants from various pretreatments were added to unpolarized macrophages (AMs). The β-galactosidase staining of AM (Fig. 4b-c) and the marker of cell senescence (Fig. 4d-f) revealed a marked improvement under co-culture with VEGF-EV-AAV/MSC-Exo@FHCCgel. The excessive inflammatory state of chronic wounds, accompanied by lipid peroxidation, enzyme deactivation and DNA damage [44], are closely associated with the excess presence of peroxides. Macrophages (Møs) intrinsically linked to inflammation are the most formidable

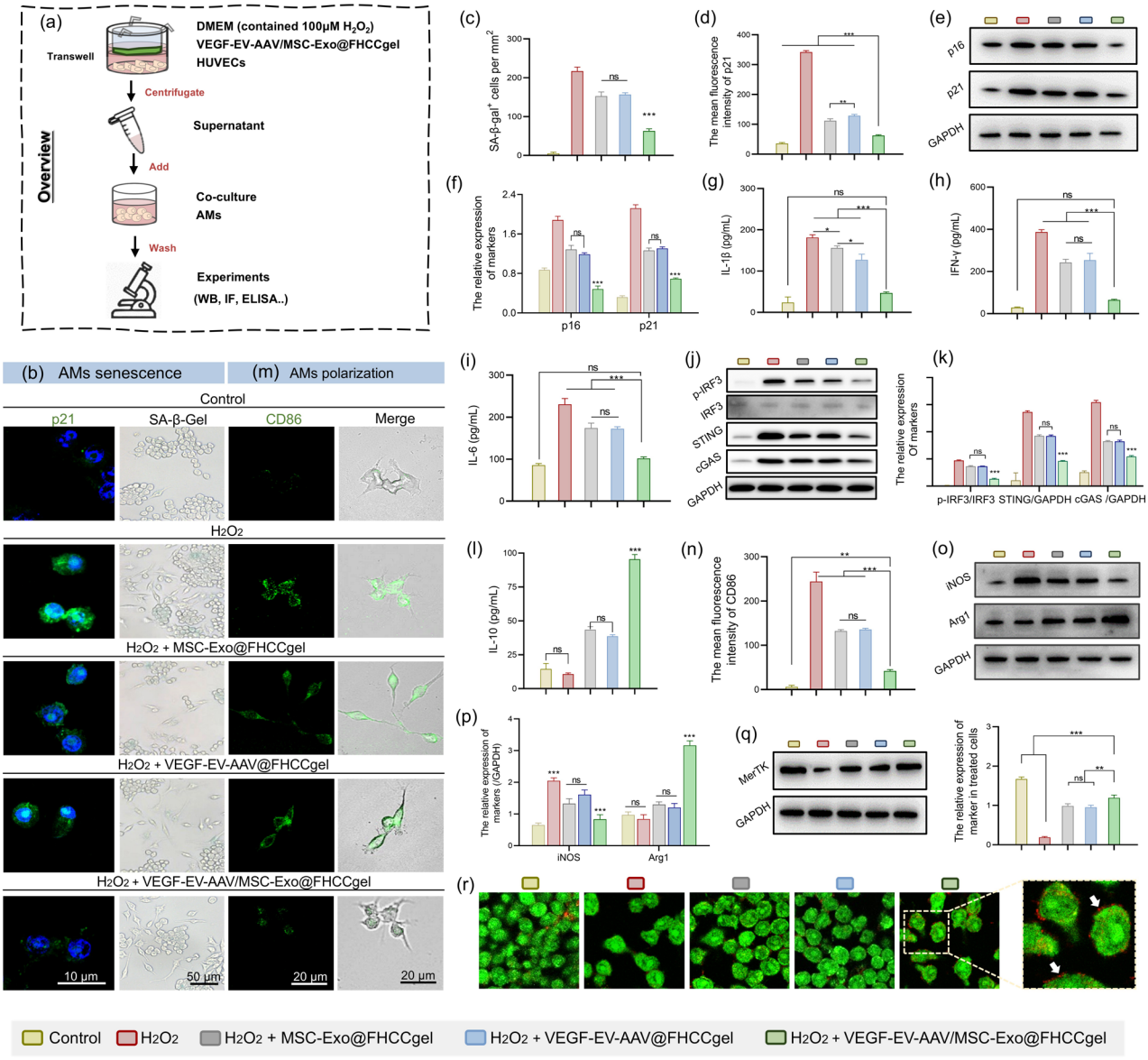

Fig. 4 Modulation of macrophage senescence and augmentation of efferocytosis by VEGF-EV-AAV/MSC-Exo@FHCCgel. (**a**) Overview of co-culture experiments. (**b**) Assessment of macrophage senescence via p21 immunofluorescence and SA-β-gal staining, along with (**c-d**) the corresponding analytical data. (**e-f**) Western blotting of cell senescence-related marker proteins and the corresponding data quantification. (**g-i**) ELISA quantification of pro-inflammation-associated factors in macrophages treated with H_2O_2. (**j-k**) Western blotting and subsequent data quantification pertaining to the proteins involved in the cGAS/STING signaling pathway. (**l**) ELISA The content of anti-inflammation-associated factor *IL-10* in macrophages treated with H_2O_2. (**m**) Representative confocal laser scanning microscopy (CLSM) images illustrating the intensity and morphology of the M1-specific marker CD86 in co-cultured M0 phenotype macrophages, and (**n**) the relative fluorescence intensity. (**o**) Western blot analysis for proteins related to M1 or M2-specific markers (iNOS and Arg1) and (**p**) corresponding statistical analysis. (**q**) Western blot analysis for proteins related to efferocytosis and corresponding statistical analysis. (**r**) The phagocytic was assessed by immunofluorescence. Evaluation of efferocytic capability through co-incubation of macrophages (Red) with apoptotic HUVECs (Green; ACs). Error bars represent the mean ± standard deviation for a sample size of $n = 3$. Statistical significance denoted as n.s.=not significant, $^{*}p < 0.05$, $^{**}p < 0.01$, and $^{***}p < 0.001$

phagocytic cells, whose aging are reciprocally led by inflammation. ELISA assays detected the reduction in the senescence-associated secretory phenotype (SASP) in the AMs culture supernatant (Fig. 4g-i).

Recent researches indicate that as intracellular DNA damage accumulates, including mitochondrial DNA (mtDNA), it may increase pathological senescence through the activation of the cGAS-STING pathway, known as "inflammatory aging" (inflammaging) [45, 46]. As expected, western blot analysis indicated significant activation of the cGAS-STING pathway in the H_2O_2-treated macrophages, while this pathway was notably inhibited in the VEGF-EV-AAV/MSC-Exo@FHCCgel group (Fig. 4j-k). This correlates with results from Fig. 3 showing a reduction in the release of Ox-mtDNA into the supernatant by HUVECs, suggesting that AMs reduce the activation of the cGAS-STING pathway due to decreased phagocytosis of Ox-mtDNA, thereby mitigating senescence. Interestingly, increase of the anti-inflammatory cytokine *IL-10* (Fig. 4l) and decrease of the pro-inflammatory cytokines *IL-6*, *IL-1β* and *IFN-γ* (Fig. 4g-i) were observed in the secretion levels, leading us to hypothesize that the polarization state of AMs in the oxidative microenvironment also underwent changes. Utilizing CD86 staining (a marker for the M1 phenotype), CLSM images revealed that AMs in the H_2O_2 group were polarized towards the M1 phenotype, whereas both the immunofluorescence intensity and cells' morphology showed no significant characteristics of M1 polarization in the VEGF-EV-AAV/MSC-Exo@FHCCgel group (Fig. 4m-n). The relative expression of iNOS (M1 marker) and Arg1 (M2 marker) also confirmed that co-culturing VEGF-EV-AAV/MSC-Exo@FHCCgel can induce the polarization of AMs towards the M2 anti-inflammatory type in an oxidative micro-environment (Fig. 4o-p). What's more, as shown in Figure S7a and d, after staining with β-actin, macrophages showed cellular elongation in cell morphology, while M2 macrophages showed a rounded morphology. Meanwhile, immunofluorescence analysis confirmed the upregulation of CD206, revealing that VEGF-EV-AAV/MSC-Exo@FHCC gel can induce the polarization of AMs towards M2 subtypes. Furthermore, flow cytometric evaluation also confirmed the transitions towards M2 subtypes (Figure S7b-c and S7e-f). Additionally, we measured the expression of γ-H2AX, a sensitive marker of DNA double-strand breaks, which reflects DNA damage during the DNA repair process. As shown in our CLSM images, ROS generated by H_2O_2 treatment significantly increased γ-H2AX levels at 24 h, indicating nuclear DNA damage (nDNA). However, with extended incubation (at 72 h), γ-H2AX expression decreased, suggesting partial self-repair of nDNA damage over time (Figure S8a). Furthermore, after applying VEGF-EV-AAV/MSC-Exo@FHCC gel, γ-H2AX expression declined as early as 24 h, indicating that this treatment accelerated nDNA repair (Figure S8b). PicoGreen staining for DNA damage yielded similar results (Figure S8c). These observations suggest that, under in vitro conditions, ECs can sustain nuclear DNA damage but are capable of partial self-repair within a certain timeframe, and VEGF-EV-AAV/MSC-Exo@FHCC gel can further enhance this repair process. Building on these findings, our current study focused on mitochondrial DNA (mtDNA) damage and Ox-mtDNA, which we found to be more susceptible to oxidative stress and less capable of repair compared to nuclear DNA. Notably, VEGF-EV-AAV/MSC-Exo@FHCC gel reversed mitoDNA damage and promoted mitoDNA repair, suggesting a unique mechanism wherein mitochondrial function and ox-mtDNA damage are mitigated by this intervention. Consequently, in this study, we concentrated on the mitochondrial dysfunction and ox-mtDNA damage mechanisms instead of exploring nDNA damage. We intend to conduct a more comprehensive investigation into this aspect in our future studies.

Mø senescence is a double-edged sword in both regulation of local inflammatory activation through cell cycle inhibition and differential polarization, and sensitively reducing its phagocytic activity to decrease the accumulation of aging signals. Phagocytic activity refers to the orderly disintegration and engulfment of cells during the autophagy process, serving as a crucial mode of cell death. This function plays a significant role in defending against viruses and maintaining intercellular balance. Western blot results from Fig. 4q indicated a significant downregulation of the efferocytosis-related marker protein MerTK following co-culture with VEGF-EV-AAV/MSC-Exo@FHCCgel. CLSM images demonstrated that AMs in the VEGF-EV-AAV/MSC-Exo@FHCCgel group could restore phagocytosis of Did-stained apoptotic HUVECs (ACs), while the proportion of ACs phagocytized by AMs in the H_2O_2 group was significantly lower (Fig. 4r). These findings suggested that as a gene delivery system with antioxidative properties, VEGF-EV-AAV/MSC-Exo@FHCCgel can protect the biological activity of VEGF-EV-AAV to efficiently transfect cells. Additionally, it synergistically regulates the interplay between endothelial cell damage and the release of inflammatory factors by macrophages, inhibiting Mø senescence and restoring efferocytosis.

Improvement of endothelial cells proliferation and angiogenesis capacity

With the improvement of the inflammatory microenvironment mediated by macrophage polarization towards the M2 phenotype, we further verified that endothelial cells exhibit enhanced proliferation and anti-apoptotic effects. Endothelial cells are critical cellular components

of the vascular wall. In both normal and pathological states, the survival of endothelial cells is essential for maintaining the integrity and functionality of blood vessels, with wound healing dependent on the degree of underlying vascularization. Vascular Endothelial Growth Factor (VEGF) serves as a crucial signaling protein, activating the PI3K/Akt signaling pathway to counteract endothelial cell apoptosis [47, 48]. Additionally, VEGF enhances the expression of protective molecules in endothelial cells, such as Bcl-2 and other anti-apoptotic proteins, thereby further preventing cell death [49]. VEGF improves the resistance of endothelial cells to apoptotic stimuli [50], such as hypoxia or inflammatory environments, making the endogenous enhancement of VEGF's anti-apoptotic activity a key objective of this study.

To elevate the endogenous expression and secretion of VEGF in endothelial cells, we innovatively developed a gene delivery system, VEGF-EV-AAV/MSC-Exo@FHCCgel. To simulate the inflammatory microenvironment of chronic wounds, 100 μM H_2O_2 was added to the culture medium [51, 52]. Cell scratch assay revealed that HUVECs co-cultured with VEGF-EV-AAV/MSC-Exo@FHCCgel migrated significantly faster than those in the VEGF-AAV/MSC-Exo@FHCCgel and H_2O_2 groups (Fig. 5a and e). F-actin staining of the cytoskeleton, observed in Fig. 3b and f, showed enhanced spread and accelerated proliferation of HUVECs under co-cultivation. Further analysis of the components of the gene delivery system that contribute to the enhanced proliferative and migratory effects revealed that both VEGF-EV-AAV and MSC-Exo could reduce intracellular ROS levels, without significant differences (Fig. 5c and g). Moreover, in the presence of H_2O_2, the improvement of endogenous VEGF regulated by VEGF-EV-AAV/MSC-Exo@FHCCgel was more than VEGF-AAV/MSC-Exo@FHCCgel (Fig. 5d). Specifically, compared with the other groups with H_2O_2 treated, proliferative activity in the VEGF-AAV/MSC-Exo@FHCCgel group increased via EDU assay (Fig. 5h). These results confirm that, within an oxidative microenvironment, the gene delivery system upregulated VEGF from HUVECs to promote proliferation and cell migration.

Diabetic wound repair promotion via facilitating vascularization

The superior transfection efficiency and antioxidative properties of the biomimetic gene delivery system in vitro inspired further investigation into its capability for diabetic wound healing (Fig. 6a). Full-thickness skin wounds (diameter 0.8 cm) were symmetrically created along the spine on the dorsal side of diabetic mice, and randomly divided into four groups: (i) Sham; (ii) MSC-Exo@FHCCgel; (iii) VEGF-EV-AAV@FHCCgel; (iv) VEGF-EV-AAV/MSC-Exo@FHCCgel. To monitor the healing process, photographs were taken periodically post-implantation, and the ulcer areas were calculated based on these images (Fig. 6b). A systematic and comprehensive understanding of the interactions between cells and the matrix is essential to promote their clinical applications in vivo. Here, we utilize an established dynamic temperature-sensitive hydrogel system for gene delivery, delving into the cellular biological responses and signaling pathways involved in chronic wound applications, which will aid in expanding its applications in the future. We included a separate group for the application of the hydrogel system to observe its promoting effects on wound healing and to exclude the influence of the hydrogel, clarifying the roles of MSC-Exo and VEGF-EV-AAV in regulating cell anti-apoptosis. As shown in Fig. 6l and n, the VEGF-EV-AAV/MSC-Exo@FHCCgel group exhibited the fastest recovery, achieving 100% healing by day 10, while the Sham group still showed wound swelling with complete healing only by day 20. Both the MSC-Exo@FHCCgel and VEGF-EV-AAV@FHCCgel groups also demonstrated healing effects, with healing times of 15 and 16 days, respectively. The above results demonstrated that the hydrogel itself has a clear promoting effect on healing, while the FHCCgel loaded with MSC-Exo and VEGF-EV-AAV synergistically enhances their respective anti-inflammatory and wound-healing effects.

For further exploration of tissue-level skin reconstruction post-treatment, wound area tissues were collected for systematic histological studies, utilizing Hematoxylin and Eosin (H&E) staining. From the H&E stained sections, we observed that the region implanted with VEGF-EV-AAV/MSC-Exo@FHCCgel had thicker epidermal and dermal layers (Fig. 6c). To ascertain the levels of vascularization post different treatments, content of VEGF in VEGF-EV-AAV/MSC-Exo@FHCCgel group was highest (Fig. 6d-i), while FHCCgel-treated tissue was higher than Sham confirming hydrogel system could promote vascularization.No significant vascularization was observed in the PBS group tissues, while vascular marker expression in the VEGF-EV-AAV@FHCCgel and MSC-Exo@FHCCgel groups were distinctly higher, though not as pronounced as in the VEGF-EV-AAV/MSC-Exo@FHCCgel group. Tissues from day 14 were stained for CD31 immunofluorescence (Fig. 6j and p). In Fig. 6k, vascular generation consistent with microscopic observations could be seen on day 21 in healed skin sublayers, with vascularization in the VEGF-EV-AAV/MSC-Exo@FHCCgel group approaching that of normal tissue. Combined with ELISA tests, this demonstrates that VEGF-EV-AAV can still enhance local VEGF levels through efficient transfection in vivo. Moreover, collagen and vascular regeneration, crucial indicators of tissue recovery [53], are noted as being more uniform and orderly in the dermal tissue of this group, with no significant inflammation,

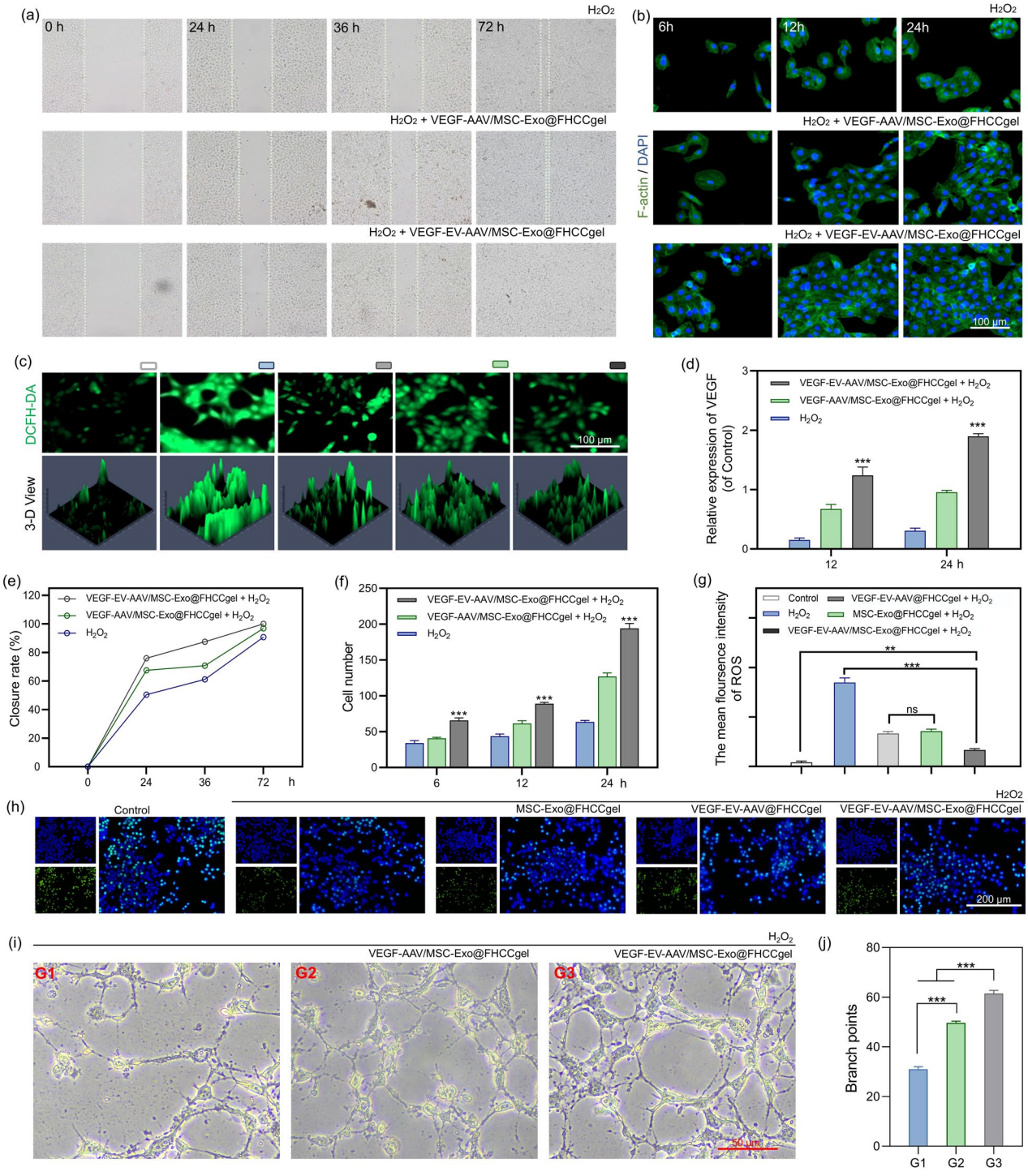

Fig. 5 Assessment of HUVECs proliferation and migration in co-culture with VEGF-EV-AAV/MSC-Exo@FHCCgel under simulated hyperoxic conditions. (**a**) Wound scratch assay demonstrating the migration of endothelial cells (ECs). (**b**) Confocal laser scanning microscopy (CLSM) images depicting the transfection of endothelial cells with F-actin/DAPI staining to evaluate cell number and morphology. (**c**) CLSM imaging for the assessment of intracellular reactive oxygen species (ROS) in ECs pre- and post-incubation with H_2O_2 across various treatments. (**d**) Relative expression levels of vascular endothelial growth factor (VEGF). (**e**) The corresponding quantification of closure rates of wound scratch assay. (**f**) Quantitative analysis of cell counts of F-actin/DAPI staining. (**g**) Statistical evaluation of ROS intensity within ECs. (**h**) EDU level of HUVECs under the oxidative culture conditions described above. (**i**) The tube formation assay to assess the ability of vascularization promotion, and (**j**) relative analysis. Error bars represent mean ± standard deviation, with $n = 3$ experiments conducted. Statistical notations: n.s.=not significant, $^{**}p < 0.01$, $^{***}p < 0.001$, indicating levels of statistical significance

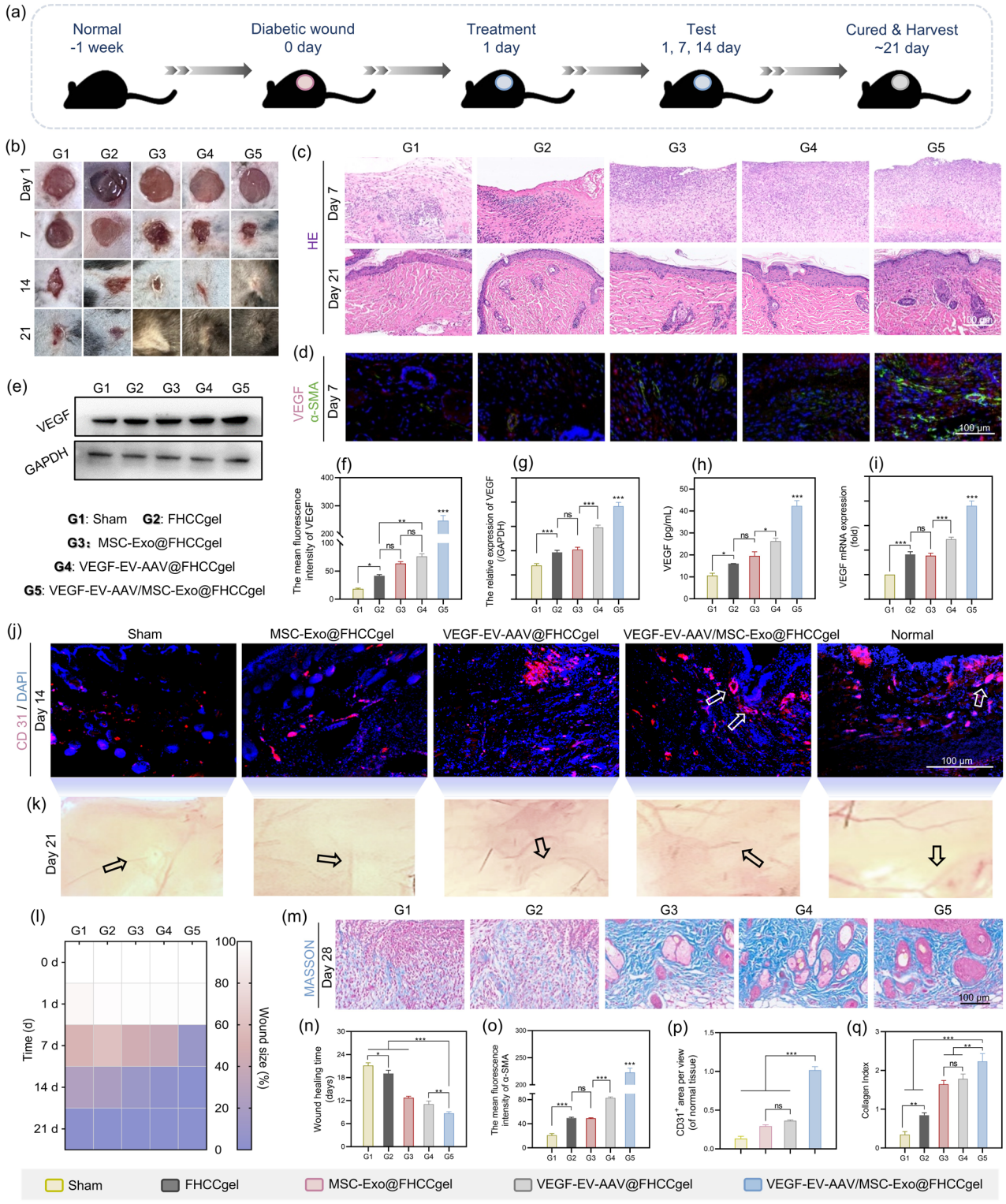

Fig. 6 (See legend on next page.)

(See figure on previous page.)

Fig. 6 Enhancement of Vascularization and Healing in Diabetic Wounds through VEGF-EV-AAV/MSC-Exo@FHCCgel Treatment by Augmenting VEGF Expression. (**a**) Schematic representation of the animal experiment protocol. (**b**) Photographic documentation of diabetic wounds following various treatments on days 0, 1, 7, and 14. Immunohistochemical analysis using (**c**) hematoxylin and eosin (HE) on days 7 and 14. (**d**) Immunofluorescence (IF) staining for α-SMA (green) and VEGF (red). (**e**) Western blotting of VEGF in wound tissues. (**f-g**) The statistical evaluations of VEGF. (**h**) ELISA and (**i**) PCR assays for detection of VEGF in wound tissues. (**j**) IF images of CD31. (**k**) Examination of newly healed skin under illumination on day 21 to assess subcutaneous vascularization. (**l**) The comparison of wound size ratios in different groups on days 0, 1, 7, and 14. (**m**) Masson's trichrome staining of diabetic wounds harvested on day 28 where the blue intensity showed the arrangement and the concentration of collagen deposition. (**n**) The corresponding analysis of wound healing time on days 0, 1, 7, and 14. Corresponding statistical analysis of (**o**) α-SMA and (**p**) CD31 IF images. (**q**) The collagen index was calculated according to Masson's trichrome staining. Error bars represent the mean ± standard deviation, with $n = 3$. Statistical significance is indicated by $^{*}p < 0.05$, $^{**}p < 0.01$, and $^{***}p < 0.001$

resembling characteristics of healthy tissue (Fig. 6m and q). It is worth mentioning that MSC-Exo promotes vascularization to some extent, but it is less effective than VEGF-EV-AAV, which suggests that the elevation of endogenous VEGF is crucial for base vascularization of diabetic wounds.

Implantation of the biomimetic gene delivery system in vivo reshapes the inflammation microenvironment

In diabetic mice, a systemic hyperglycemic and hyperoxidative microenvironment disrupts homeostatic mechanisms, leading to impaired wound healing. However, the molecular pathways that mediate aberrant inflammatory signaling remain unclear. Here, we further validated that VEGF-EV-AAV/MSC-Exo@FHCCgel promoted MerTK signaling involved in efferocytosis and increase the M2 phenotype macrophages in vivo by inhibiting the cGAS-STING pathway. Western blot (WB) analysis indicated that the expression of proteins related to the cGAS-STING pathway in the wound tissues implanted with VEGF-EV-AAV/MSC-Exo@FHCCgel was significantly lower than in other groups (Fig. 7a-b), and the expression of the efferocytosis-related receptor MerTK was highest (Fig. 7c-d). We speculate that the elevation of endogenous VEGF induced by VEGF-EV-AAV and the release of MSC-Exo both contribute to the enhancement of local efferocytosis to some extent.

Furthermore, wound tissues with different treatment were digested to obtained single-cell, and labeled with CD86 and CD206. Flow cytometry (Fig. 7e-h) and immunofluorescence staining (Figure S9) analysis revealed that, compared with other groups, anti-inflammatory M2 phenotype macrophages were significantly infiltrated in the VEGF-EV-AAV/MSC-Exo@FHCCgel-treated tissue, whereas pro-inflammatory M1 phenotype macrophages infiltrated in the control tissue (Fig. 7e-h). Interestingly, compared to other groups, the wound implanted with VEGF-EV-AAV/MSC-Exo@FHCCgel displayed more complete skin appendages on day 28. Recent studies suggest that skin is highly sensitive to resident regulatory T cells (Tregs), which play a crucial role in maintaining local immune balance in the skin [54]. Therefore, we explored the involvement of Tregs in promoting tissue repair following the remodeling of the inflammatory microenvironment of the wound. Increased infiltration of Tregs in the wound tissue of the VEGF-EV-AAV/MSC-Exo@FHCCgel group via immunofluorescence staining (Fig. 7i-j). Similarly, flow cytometry identified that the proportion of Foxp3+/CD25 + cells in this group was significantly higher than in other groups (Fig. 7k-l). The transcription levels of anti-inflammatory factors in the VEGF-EV-AAV/MSC-Exo@FHCCgel group were significantly higher than those of pro-inflammatory factors in other groups (Fig. 7m-p).

Our findings identify the cGAS-STING pathway as a driver of the crosstalk between senescence and inflammation in chronic wounds and demonstrate that VEGF-EV-AAV/MSC-Exo@FHCCgel is a potential strategy to disrupt this deleterious cycle. On one hand, downregulating the cGAS-STING signaling that mediates DNA immune sensing restores local efferocytosis to clear necrotic material and induces macrophage polarization to an anti-inflammatory M2 phenotype, releasing anti-inflammatory factors and preventing ongoing inflammation. On the other hand, improving tissue senescence, reducing the expression of senescence-associated secretory phenotype (SASP), alleviates senescence-related inflammation in diabetic wounds, and enhances Treg-mediated skin repair functions.

Conclusion

In summary, this study developed a purified extracellular vesicle-encapsulated AAV (EV-AAV) from HEK293T cells using a two-step ultrapurification method based on Iodixanol, and constructed an implantable 3D tissue-engineered bionic scaffold, VEGF-EV-AAV/MSC-Exo@FHCCgel, based on optimized thermosensitive hydrogel. As the previous researches shown, hydrogels are highly versatile platforms with a wide range of biomedical applications. Despite recent advancements in EV research, composite hydrogels are typically used immediately after preparation, lacking established storage methods and validation of EV activity. To address this, this study developed an EV-AAV hydrogel system aimed at providing dual protection for both AAV and EVs [55–57]. In general, cells perceive surrounding material cues and transduce these signals into intracellular biochemical signals, thereby affecting cell viability, gene expression,

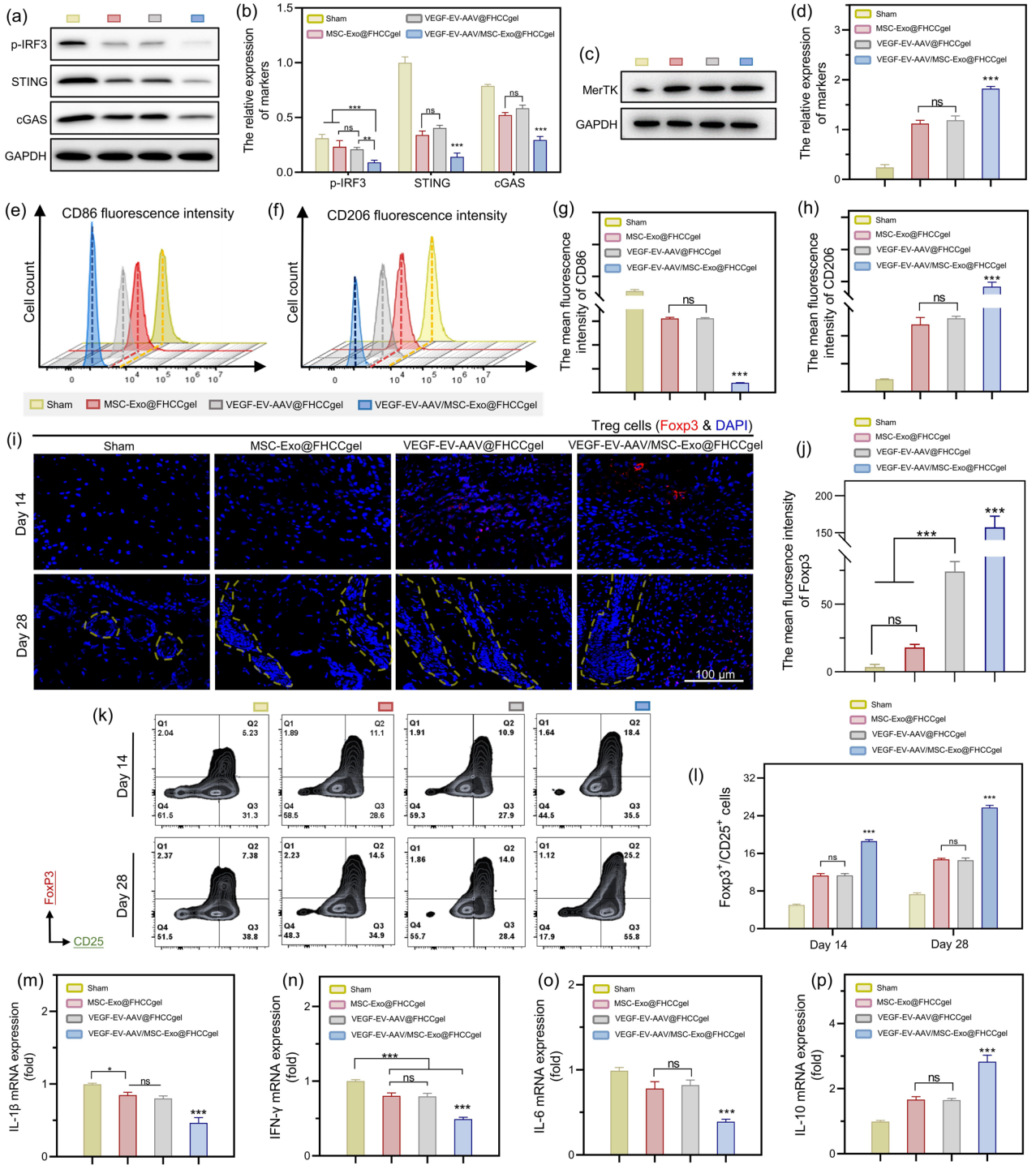

Fig. 7 Immunomodulatory Effects and Enhanced Wound Healing Induced by VEGF-EV-AAV/MSC-Exo@FHCCgel in Diabetic Wounds. This formulation ameliorated immune dysregulation and fostered effective wound repair. Western blot analyses were conducted to assess protein levels within (**a-b**) the cGAS/STING and (**c-d**) efferocytosis signaling pathways in skin tissues extracted from mice with varied treatments. (**e-h**) Flow cytometric evaluation and associated quantitative analysis of emerging tissue markers for CD86 (indicative of M1 macrophages) and CD206 (indicative of M2 macrophages) at day 3. (**i**) Immunofluorescence staining for Foxp3 (a Treg marker) on days 14 and 28, accompanied by (**j**) corresponding statistical analysis. (**k-l**) Flow cytology sorted $CD25^+/Foxp3^+$ cells picked, and relative analysis. (**m-p**) Quantitative PCR was employed to measure transcript levels of inflammatory mediators in wound tissues on day 7 post-treatment. Error bars represent the mean ± standard deviation, with $n = 3$. Statistical significance is denoted by $^{**}p < 0.01$, $^{***}p < 0.001$, and n.s.=not significant

and cell lineage specification. A systematic and comprehensive understanding of the interactions between cells and the matrix is essential to promote their clinical applications in vivo. Here, we utilize an established dynamic temperature-sensitive hydrogel system for gene delivery, delving into the cellular biological responses and signaling pathways involved in chronic wound applications, which will aid in expanding its applications in the future. This hydrogel system serves as a gene delivery system for the sustained release of VEGF-bearing EV-AAVs and anti-inflammatory MSC-Exos. Protected by the extracellular vesicles, the VEGF-EV-AAVs efficiently transfect endothelial cells, enhancing the expression of endogenous VEGF. In fact, existing research indicates that both MSC-Exo [58] and VEGF [59] can improve intracellular oxidative stress damage and promote the proliferation of endothelial cells, which has been consistently validated in this article. In vivo and in vitro experiments confirmed that the antioxidant effects of VEGF-EV-AAV/MSC-Exo@FHCCgel were superior to those of VEGF-EV-AAV@FHCCgel and MSC-Exo@FHCCgel. The timely closure of mitochondrial membrane pores in endothelial cells reduces the extracellular leakage of oxidized mitochondrial DNA (Ox-mtDNA). Concurrently, macrophages reduce the ingestion of Ox-mtDNA, inhibiting the cGAS/STING pathway and improving cellular senescence. A reduction in senescence-associated secretory phenotype (SASP) facilitates polarization towards an anti-inflammatory M2 phenotype in macrophages, effectively preventing a new cycle of inflammation. Accompanied by a decrease in local inflammatory factors, Treg cell infiltrating and function enhancing aids the basal layer remodel in wound bed. This work provides evidence for the novel concept of combining EV-AAV with tissue engineering as a gene delivery system for treating diabetic wounds. We also believe that this integrated design of anti-inflammatory regulation and vascular regeneration will inspire strategies for endogenous repair of chronic wounds.

Supplementary Information

The online version contains supplementary material available at https://doi.org/10.1186/s12951-025-03261-w.

Supplementary Material 1

Acknowledgments

This work was supported by Instrumentation and Service Center for Science and Technology, Beijing Normal University, Zhuhai. The characterization results were supported by Beijing Zhongkebaice Technology Service Co., Ltd.（www.zkbaice.cn）

Author contributions

Li Zhiqing, Liang Yaxuan and Huang Cong funded and supervised the research and experimental procedures; He Shan, Li Zhenhao, Xie Lei, Lin Rongtian and Yan Biying jointly conducted the experiments and performed data analysis; He Shan primarily wrote the manuscript; Li Bixiang, Luo Lingxi, Xu Youshan, and Wen Huangding participated in the experiments. All authors reviewed the manuscript.

Funding

This research was supported, in whole or in part, by the National Natural Science Foundation of China (Zhiqing Li, Grant Number 82472556), GuangDong Basic and Applied Basic Research Foundation (Zhiqing Li, Grant Number 2024A1515012825; Cong Huang, Grant Number 2023A1515220192) and National College Students Innovation and Entrepreneurship Training Program (Shan He and Zhiqing Li, Grant Number 202312121032).

Data availability

No datasets were generated or analysed during the current study.

Declarations

Ethics approval and consent to participate

The care and use of all animals were approved by Laboratory Animal Ethics Committee of Nanfang hospital, Southern Medical University, Guangdong Province, China (approval number: IACUC-LAC-20221015-001) and was strictly compliant with the Guide for the Care and Use of Laboratory Animals of the National Institutes of Health.

Consent for publication

All authors have provided consent for the manuscript to be published.

Competing interests

The authors declare no competing interests.

Author details

[1]Department of Burns, Nanfang Hospital, Southern Medical University, Guangzhou 510515, China
[2]Department of Ultrasound, The First Affiliated Hospital of Shantou University Medical College, Shantou 515041, China
[3]Department of Biology, Faculty of Arts and Sciences, Beijing Normal University at Zhuhai, Zhuhai 519087, China
[4]Department of General Surgery, Nanfang Hospital, Southern Medical University, Guangzhou 510515, China
[5]Department of Radiology, The Cancer Hospital of Shantou University Medical College, Shantou, Guangdong 515041, China
[6]R&D Center, Guangdong Luofushan Sinopharm Co., Ltd., Huizhou 516100, China
[7]The First School of Clinical Medicine, Southern Medical University, Guangzhou 510515, China
[8]Huiqiao Medical Center (International Medical Service), NanFang Hospital, Southern Medical University, Guangzhou 510515, China
[9]Center for Biological Science and Technology, Key Laboratory of Cell Proliferation and Regulation Biology of Ministry of Education, Zhuhai-Macao Biotechnology Joint Laboratory, Beijing Normal University at Zhuhai, Zhuhai 519087, China

Received: 7 November 2024 / Accepted: 20 February 2025
Published online: 24 March 2025

References

1. Lee J, van der Valk WH, Serdy SA, Deakin C, Kim J, Le AP, Koehler KR. Generation and characterization of hair-bearing skin organoids from human pluripotent stem cells. Nat Protoc. 2022;17(5):1266–305.
2. Matoori S, Veves A, Mooney DJ. Advanced bandages for diabetic wound healing. Sci Transl Med. 2021;13(585).
3. Sharifiaghdam M, Shaabani E, Faridi-Majidi R, De Smedt SC, Braeckmans K, Fraire JC. Macrophages as a therapeutic target to promote diabetic wound healing. Mol Therapy: J Am Soc Gene Therapy. 2022;30(9):2891–908.
4. Dixon D, Edmonds M. Managing diabetic foot ulcers: pharmacotherapy for wound healing. Drugs. 2021;81(1):29–56.
5. Chang M, Nguyen TT. Strategy for treatment of infected diabetic foot ulcers. Acc Chem Res. 2021;54(5):1080–93.
6. Uemura A, Fruttiger M, D'Amore PA, De Falco S, Joussen AM, Sennlaub F, Brunck LR, Johnson KT, Lambrou GN, Rittenhouse KD, Langmann T. VEGFR1

signaling in retinal angiogenesis and microinflammation. Prog Retin Eye Res. 2021;84:100954.
7. Jaipersad AS, Lip GY, Silverman S, Shantsila E. The role of monocytes in angiogenesis and atherosclerosis. J Am Coll Cardiol. 2014;63(1):1–11.
8. Daseke MJ 2nd, Tenkorang MAA, Chalise U, Konfrst SR, Lindsey ML. Cardiac fibroblast activation during myocardial infarction wound healing: fibroblast polarization after MI. Matrix Biology: J Int Soc Matrix Biology. 2020;91–2:109–116.
9. Ginn SL, Amaya AK, Alexander IE, Edelstein M, Abedi MR. Gene therapy clinical trials worldwide to 2017: an update. J Gene Med. 2018;20(5):e3015.
10. Smith RH. Adeno-associated virus integration: virus versus vector. Gene Ther. 2008;15(11):817–22.
11. Niwano K, Arai M, Koitabashi N, Watanabe A, Ikeda Y, Miyoshi H, Kurabayashi M. Lentiviral vector-mediated SERCA2 gene transfer protects against heart failure and left ventricular remodeling after myocardial infarction in rats. Mol Therapy: J Am Soc Gene Therapy. 2008;16(6):1026–32.
12. Ribeil JA, Hacein-Bey-Abina S, Payen E, Magnani A, Semeraro M, Magrin E, Caccavelli L, Neven B, Bourget P, Nemer WE, Bartolucci P, Weber L, Puy H, Meritet JF, Grevent D, Beuzard Y, Chrétien S, Lefebvre T, Ross RW, Negre O, Veres G, Sandler L, Soni S, de Montalembert M, Blanche S, Leboulch P, Cavazzana M. Gene therapy in a patient with sickle cell disease. N Engl J Med. 2017;376(9):848–55.
13. Rangarajan S, Walsh L, Lester W, Perry D, Madan B, Laffan M, Yu H, Vettermann C, Pierce GF, Wong WY, Pasi KJ. AAV5-Factor VIII gene transfer in severe hemophilia A. N Engl J Med. 2017;377(26):2519–30.
14. Greenberg B, Butler J, Felker GM, Ponikowski P, Voors AA, Desai AS, Barnard D, Bouchard A, Jaski B, Lyon AR, Pogoda JM, Rudy JJ, Zsebo KM. Calcium upregulation by percutaneous administration of gene therapy in patients with cardiac disease (CUPID 2): a randomised, multinational, double-blind, placebo-controlled, phase 2b trial. Lancet (London England). 2016;387(10024):1178–86.
15. Jessup M, Greenberg B, Mancini D, Cappola T, Pauly DF, Jaski B, Yaroshinsky A, Zsebo KM, Dittrich H, Hajjar RJ. Calcium upregulation by percutaneous administration of gene therapy in cardiac disease (CUPID): a phase 2 trial of intracoronary gene therapy of sarcoplasmic reticulum Ca2+-ATPase in patients with advanced heart failure. Circulation. 2011;124(3):304–13.
16. Valdmanis PN, Lisowski L, Kay MA. rAAV-mediated tumorigenesis: still unresolved after an AAV assault. Mol Therapy: J Am Soc Gene Therapy. 2012;20(11):2014–7.
17. Louis Jeune V, Joergensen JA, Hajjar RJ, Weber T. Pre-existing anti-adeno-associated virus antibodies as a challenge in AAV gene therapy. Hum Gene Therapy Methods. 2013;24(2):59–67.
18. Wang Z, Zhu T, Qiao C, Zhou L, Wang B, Zhang J, Chen C, Li J, Xiao X. Adeno-associated virus serotype 8 efficiently delivers genes to muscle and heart. Nat Biotechnol. 2005;23(3):321–8.
19. Tang Q, Lu B, He J, Chen X, Fu Q, Han H, Luo C, Yin H, Qin Z, Lyu D, Zhang L, Zhou M, Yao K. Exosomes-loaded thermosensitive hydrogels for corneal epithelium and stroma regeneration. Biomaterials. 2022;280:121320.
20. Bialik M, Kuras M, Sobczak M, Oledzka E. Achievements in thermosensitive gelling systems for rectal administration. Int J Mol Sci. 2021;22(11).
21. Dethe MR, Ahmed PAH, Agrawal M, Roy U, Alexander A. PCL-PEG copolymer based injectable thermosensitive hydrogels. J Control Release. 2022;343:217–36.
22. Aliakbari F, Marzookian K, Parsafar S, Hourfar H, Nayeri Z, Fattahi A, Raeiji M, Boroujeni NN, Otzen DE, Morshedi D. The impact of hUC MSC-derived exosome-nanoliposome hybrids on α-synuclein fibrillation and neurotoxicity. Sci Adv. 2024;10(14):eadl3406.
23. Guo G, Tan Z, Liu Y, Shi F, She J. The therapeutic potential of stem cell-derived exosomes in the ulcerative colitis and colorectal cancer. Stem Cell Res Ther. 2022;13(1):138.
24. Yang S, Liang X, Song J, Li C, Liu A, Luo Y, Ma H, Tan Y, Zhang X. A novel therapeutic approach for inflammatory bowel disease by exosomes derived from human umbilical cord mesenchymal stem cells to repair intestinal barrier via TSG-6. Stem Cell Res Ther. 2021;12(1):315.
25. Bi Y, Qiao X, Liu Q, Song S, Zhu K, Qiu X, Zhang X, Jia C, Wang H, Yang Z, Zhang Y, Ji G. Systemic proteomics and MiRNA profile analysis of exosomes derived from human pluripotent stem cells. Stem Cell Res Ther. 2022;13(1):449.
26. Zhang Z, Mi T, Jin L, Li M, Zhanghuang C, Wang J, Tan X, Lu H, Shen L, Long C, Wei G, He D. Comprehensive proteomic analysis of exosome mimetic vesicles and exosomes derived from human umbilical cord mesenchymal stem cells. Stem Cell Res Ther. 2022;13(1):312.
27. Yang K, Li D, Wang M, Xu Z, Chen X, Liu Q, Sun W, Li J, Gong Y, Liu D, Shao C, Liu Q, Li X. Exposure to blue light stimulates the proangiogenic capability of exosomes derived from human umbilical cord mesenchymal stem cells. Stem Cell Res Ther. 2019;10(1):358.
28. Cao T, Chen H, Huang W, Xu S, Liu P, Zou W, Pang M, Xu Y, Bai X, Liu B, Rong L, Cui ZK, Li M. hUC-MSC-mediated recovery of subacute spinal cord injury through enhancing the pivotal subunits B3 and Γ2 of the GABA(A) receptor. Theranostics. 2022;12(7):3057–78.
29. Lu T, Zhang J, Cai J, Xiao J, Sui X, Yuan X, Li R, Li Y, Yao J, Lv G, Chen X, Chen H, Zeng K, Liu Y, Chen W, Chen G, Yang Y, Zheng J, Zhang Y. Extracellular vesicles derived from mesenchymal stromal cells as nanotherapeutics for liver ischaemia-reperfusion injury by transferring mitochondria to modulate the formation of neutrophil extracellular traps. Biomaterials. 2022;284:121486.
30. Galipeau J, Sensébé L. Mesenchymal stromal cells: clinical challenges and therapeutic opportunities. Cell Stem Cell. 2018;22(6):824–33.
31. Peng C, Trojanowski JQ, Lee VM. Protein transmission in neurodegenerative disease. Nat Reviews Neurol. 2020;16(4):199–212.
32. Deng H, Dong A, Song J, Chen X. Injectable thermosensitive hydrogel systems based on functional PEG/PCL block polymer for local drug delivery. J Control Release. 2019;297:60–70.
33. Pan W, Wu B, Nie C, Luo T, Song Z, Lv J, Tan Y, Liu C, Zhong M, Liao T, Wang Z, Yi G, Zhang L, Liu X, Li B, Chen J, Zheng L. NIR-II responsive nanohybrids incorporating thermosensitive hydrogel as sprayable dressing for Multidrug-Resistant-Bacteria infected wound management. ACS Nano. 2023;17(12):11253–67.
34. Li S, Yang C, Li J, Zhang C, Zhu L, Song Y, Guo Y, Wang R, Gan D, Shi J, Ma P, Gao F, Su H. Progress in pluronic F127 derivatives for application in wound healing and repair. Int J Nanomed. 2023;18:4485–505.
35. Chao Y, Xu L, Liang C, Feng L, Xu J, Dong Z, Tian L, Yi X, Yang K, Liu Z. Combined local immunostimulatory radioisotope therapy and systemic immune checkpoint Blockade imparts potent antitumour responses. Nat Biomedical Eng. 2018;2(8):611–21.
36. Lv Q, Wang Y, Tian W, Liu Y, Gu M, Jiang X, Cai Y, Huo R, Li Y, Li L, Wang X. Exosomal miR-146a-5p derived from human umbilical cord mesenchymal stem cells can alleviate antiphospholipid antibody-induced trophoblast injury and placental dysfunction by regulating the TRAF6/NF-κB axis. J Nanobiotechnol. 2023;21(1):419.
37. Peralta C, Jiménez-Castro MB, Gracia-Sancho J. Hepatic ischemia and reperfusion injury: effects on the liver sinusoidal milieu. J Hepatol. 2013;59(5):1094–106.
38. Jorgensen AN, Rashdan NA, Rao KNS, Delgadillo LF, Kolluru GK, Krzywanski DM, Pattillo CB, Kevil CG, Nam HW. Neurogranin expression regulates mitochondrial function and redox balance in endothelial cells. Redox Biol. 2024;70:103085.
39. Hu Z, Wang D, Gong J, Li Y, Ma Z, Luo T, Jia X, Shi Y, Song Z. MSCs deliver Hypoxia-Treated mitochondria reprogramming acinar metabolism to alleviate severe acute pancreatitis injury. Adv Sci (Weinh). 2023;10(25):e2207691.
40. Miettinen TP, Björklund M. Mitochondrial function and cell size: an allometric relationship. Trends Cell Biol. 2017;27(6):393–402.
41. Xian H, Watari K, Sanchez-Lopez E, Offenberger J, Onyuru J, Sampath H, Ying W, Hoffman HM, Shadel GS, Karin M. Oxidized DNA fragments exit mitochondria via mPTP- and VDAC-dependent channels to activate NLRP3 inflammasome and interferon signaling. Immunity. 2022;55(8):1370–e13858.
42. Chakradhar S. Puzzling over privilege: how the immune system protects-and fails-the testes. Nat Med. 2018;24(1):2–5.
43. Park EH, Kim YJ, Yamabe N, Park SH, Kim HK, Jang HJ, Kim JH, Cheon GJ, Ham J, Kang KS. Stereospecific anticancer effects of ginsenoside Rg3 epimers isolated from heat-processed American ginseng on human gastric cancer cell. J Ginseng Res. 2014;38(1):22–7.
44. Wang M, Pan W, Xu Y, Zhang J, Wan J, Jiang H. Microglia-Mediated neuroinflammation: A potential target for the treatment of cardiovascular diseases. J Inflamm Res. 2022;15:3083–94.
45. Ablasser A, Chen ZJ. cGAS in action: expanding roles in immunity and inflammation. Science. 2019;363(6431).
46. Gulen MF, Samson N, Keller A, Schwabenland M, Liu C, Glück S, Thacker VV, Favre L, Mangeat B, Kroese LJ, Krimpenfort P, Prinz M, Ablasser A. cGAS-STING drives ageing-related inflammation and neurodegeneration. Nature. 2023;620(7973):374–80.
47. Wang HJ, Ran HF, Yin Y, Xu XG, Jiang BX, Yu SQ, Chen YJ, Ren HJ, Feng S, Zhang JF, Chen Y, Xue Q, Xu XY. Catalpol improves impaired neurovascular unit in ischemic stroke rats via enhancing VEGF-PI3K/AKT and VEGF-MEK1/2/ERK1/2 signaling. Acta Pharmacol Sin. 2022;43(7):1670–85.

48. He Y, Wang H, Lin S, Chen T, Chang D, Sun Y, Wang C, Liu Y, Lu Y, Song J, Li S, Xu W, Lin Y, Zheng Y, Zhou X, Huang Q, Huang M. Advanced effect of Curcumin and Resveratrol on mitigating hepatic steatosis in metabolic associated fatty liver disease via the PI3K/AKT/mTOR and HIF-1/VEGF cascade. Biomed Pharmacother. 2023;165:115279.
49. Yamashita M, Niisato M, Kawasaki Y, Karaman S, Robciuc MR, Shibata Y, Ishida Y, Nishio R, Masuda T, Sugai T, Ono M, Tuder RM, Alitalo K, Yamauchi K. VEGF-C/VEGFR-3 signalling in macrophages ameliorates acute lung injury. Eur Respir J. 2022;59(4).
50. Meng LB, Zhang YM, Shan MJ, Qiu Y, Zhang TJ, Gong T. Pivotal micro factors associated with endothelial cells. Chin Med J. 2019;132(16):1965–73.
51. Xiong Y, Chen L, Liu P, Yu T, Lin C, Yan C, Hu Y, Zhou W, Sun Y, Panayi AC, Cao F, Xue H, Hu L, Lin Z, Xie X, Xiao X, Feng Q, Mi B, Liu G. All-in-One: multi-functional hydrogel accelerates oxidative diabetic wound healing through Timed-Release of exosome and fibroblast growth factor, small (Weinheim an der Bergstrasse. Germany). 2022;18(1):e2104229.
52. Liu K, Gao X, Hu C, Gui Y, Gui S, Ni Q, Tao L, Jiang Z. Capsaicin ameliorates diabetic retinopathy by inhibiting poldip2-induced oxidative stress. Redox Biol. 2022;56:102460.
53. Fan X, Wu X, Yang F, Wang L, Ludwig K, Ma L, Trampuz A, Cheng C, Haag R. A Nanohook-Equipped Bionanocatalyst for localized Near-Infrared-Enhanced catalytic bacterial disinfection. Angew Chem Int Ed Engl. 2022;61(8):e202113833.
54. Cohen JN, Gouirand V, Macon CE, Lowe MM, Boothby IC, Moreau JM, Gratz IK, Stoecklinger A, Weaver CT, Sharpe AH, Ricardo-Gonzalez RR, Rosenblum MD. Regulatory T cells in skin mediate immune privilege of the hair follicle stem cell niche. Sci Immunol. 2024;9(91):eadh0152.
55. Li Z, Liu J, Song J, Yin Z, Zhou F, Shen H, Wang G, Su J. Multifunctional hydrogel-based engineered extracellular vesicles delivery for complicated wound healing. Theranostics. 2024;14(11):4198–217.
56. Wang Y, Lin Q, Zhang H, Wang S, Cui J, Hu Y, Liu J, Li M, Zhang K, Zhou F, Jing Y, Geng Z, Su J. M2 macrophage-derived exosomes promote diabetic fracture healing by acting as an Immunomodulator. Bioact Mater. 2023;28:273–83.
57. Liu H, Zhang Q, Wang S, Weng W, Jing Y, Su J. Bacterial extracellular vesicles as bioactive nanocarriers for drug delivery: advances and perspectives. Bioact Mater. 2022;14:169–81.
58. Wang T, Jian Z, Baskys A, Yang J, Li J, Guo H, Hei Y, Xian P, He Z, Li Z, Li N, Long Q. MSC-derived exosomes protect against oxidative stress-induced skin injury via adaptive regulation of the NRF2 defense system. Biomaterials. 2020;257:120264.
59. Yang KJ, Choi WJ, Chang YK, Park CW, Kim SY, Hong YA. Inhibition of Xanthine oxidase protects against diabetic kidney disease through the amelioration of oxidative stress via VEGF/VEGFR Axis and NOX-FoxO3a-eNOS signaling pathway. Int J Mol Sci. 2023;24(4).

Publisher's note